Journal of
Applied Remote Sensing

# Comparison of skylight polarization measurements and MODTRAN-P calculations

Nathan J. Pust
Joseph A. Shaw

SPIE

# Comparison of skylight polarization measurements and MODTRAN-P calculations

**Nathan J. Pust and Joseph A. Shaw**
Montana State University, Department of Electrical and Computer Engineering,
610 Cobleigh Hall, Bozeman, Montana, 59717
jshaw@ece.montana.edu

**Abstract.** Increased use of polarization in optical remote sensing provides motivation for a study of instruments and methods that can be used to test and validate polarized atmospheric radiative transfer codes and simulation tools. An example comparison of measured skylight polarization and calculations from a preliminary version of the polarized MODTRAN radiative transfer code (MODTRAN-P) for cloud-free conditions is presented. The study combines data from an all-sky polarization imager at 452, 491, 532, 632, and 701 nm, a solar radiometer, a zenith-viewing aerosol and cloud lidar, a weather station, and radiosonde profiles of atmospheric temperature and pressure to compare measurements and model calculations of the maximum degree of linear polarization for cloud-free atmospheres. Comparisons for conditions ranging from extremely clear to thick forest fire smoke indicate that the additional data most needed for constraining calculations are aerosol size distributions. Nevertheless, comparisons made with standard aerosol models in version 2.1-alpha of MODTRAN-P with an unpolarized multiple-scattering algorithm illustrate the methodology and provide quantitative information about the range of conditions for which a single-scattering radiative transfer code is useful for predicting skylight polarization. This approach is also warranted because many users simulate atmospheres with the MODTRAN standard aerosol models. The agreement of model calculations with measurements is high for low aerosol optical depth and degrades with increasing optical depth. Agreement between measurements and model results is best for the longer wavelengths.  [DOI: 10.1117/1.3595686]

**Keywords:** polarization; polarimetry; atmospheric optics.

Paper 10094PRR received Jun. 23, 2010; revised manuscript received Apr. 20, 2011; accepted for publication May 3, 2011; published online Jun. 2, 2011.

## 1 Introduction

Increasing use of polarization in remote sensing[1–4] creates a corresponding need for polarized radiative transfer codes and simulation tools. This is particularly important for modeling skylight and atmospheric effects in the visible- near-infrared (VNIR) spectral range, where scattering dominates thermal emission.[5,6] In this part of the spectrum, the simple Rayleigh scattering model adequately models polarized skylight for pure molecular scattering.[7] However, including the effects of clouds, aerosols, and multiple scattering requires a more sophisticated radiative transfer model. For confident use of such tools, they must be validated with measured data. As an example, we show comparisons of measured skylight polarization and modeling results from version 2.1-alpha of the polarized MODTRAN code (MODTRAN-P) developed by the Air Force Research Laboratory.

MODTRAN is a proven atmospheric radiation transfer model that has been developed and refined for several decades.[8] The standard version of MODTRAN simulates atmospheric radiance, emission, and transmittance for ultraviolet-through-infrared wavelengths under a variety of atmospheric conditions—but does not model polarization. The new MODTRAN-P code

1931-3195/2011/$25.00 © 2011 SPIE

adds the polarization capability.[9] Although a polarized multiple scattering version is now being evaluated,[10] the early version that we possess incorporates polarized single scattering with unpolarized multiple scattering.[10,11] Although the MODTRAN-P code has yet to be released to the public officially, versions of it are in use within the community. For example, it has been used along with the DIRSIG code to predict polarized scene radiances.[12] Although members of the polarization community frequently ask for guidance on assessing the accuracy of simulations made with this and similar codes, there has been very little published previously about the mechanisms for answering such questions. The paper by Devaraj et al.[12] showed comparisons of calculations with previous measurements and Rayleigh scattering theory, with a general trend of good comparison under low-aerosol conditions, and degraded agreement with increased aerosol loading. Our study expands on this approach through a comparison of MODTRAN-P simulations with direct sky polarization measurements.

The study we report here uses a VNIR imaging polarimeter that we developed for studying both sky polarization and ground-based object polarization signatures.[13,14] Our polarimeter is capable of switching between two fields of view—a wide-angle fish eye field of view for imaging the full sky and a narrow field of view for imaging smaller objects. At the time of this study, the instrument operated in five 10-nm bands centered at 452, 491, 532, 632, and 701 nm. Two liquid crystal variable retarders (LCVRs) are used to electronically vary the retardance seen by incoming light at each wavelength so that a full Stokes image is measured in less than a few tenths of a second. (Intensity images from the camera are inverted by a calibration matrix to form the 4-element Stokes images.) Quick acquisition allows reliable measurements in partly cloudy skies without polarization artifacts that would arise if the clouds were to move between frames. The LCVR-based Stokes image retrieval is repeated for each wavelength, which is selected with a rotating filter wheel. This imager obtains polarized sky measurements with uncertainty less than (usually much less than) $\pm 3\%$ in the degree of linear polarization (DoLP).

In this paper we discuss methods for using sky polarimeter data along with lidar, solar radiometer, weather station, and radiosonde data for comparing with polarized radiative transfer model simulations. We illustrate the method with comparisons of observed maximum DoLP and MODTRAN-P predictions, and indicate the need for additional aerosol characterization for future comparisons.

## 2 Comparison Methodology

For clear-sky comparisons of measured and modeled skylight polarization, the most important variables are the aerosol and molecular vertical profiles. These parameters are discussed separately below.

### *2.1 Molecular Profiles*

Rayleigh scattering can be calculated from standard molecular profiles,[15] such as those contained within MODTRAN.[16] The primary variable is standard pressure for the observer altitude, and our comparisons suggest that $<0.5\%$ DoLP error results from using standard atmosphere models with the observer's altitude instead of radiosonde profiles and the measured surface air pressure. Absorption effects by water vapor are negligible for all the polarimeter wavelengths except the 700 nm. (This was verified by modeling.) Although inclusion of profile relative humidity is only strictly necessary at 700 nm, we used concurrent meterological data from our own radiosondes and weather station in all wavelength bands.

We also tested the model dependence on variations in molecular species other than water vapor (i.e., CO, $CO_2$, $N_2$, etc.). By changing between MODTRAN standard molecular profiles for these species in conjunction with a fixed temperature, pressure, and humidity profile from a radiosonde, we found that changes in these species only affected the modeled maximum degree of polarization by a maximum of 0.5%. When compared to errors possibly introduced

by assumptions made for other variables (like atmospheric homogeneity, aerosol optical depth, and aerosol type), this possible variation is acceptable.

### 2.2 Aerosol Extinction Profile and Scattering Phase Matrices

The primary perturbation of the observed polarization pattern from the theoretical Rayleigh scattering pattern is a result of scattering by aerosols. MODTRAN represents aerosol type and extinction using four separate aerosol classes. These four classes correspond to boundary layer aerosol, tropospheric aerosol, stratospheric aerosol, and high-stratospheric aerosol. Each of these four aerosol classes is defined by an extinction profile, wavelength dependence, and a scattering phase matrix. Each extinction profile is defined at 550 nm, while the wavelength dependence defines a scaling factor that determines the extinction for wavelengths away from 550 nm. Aerosol scattering phase matrices are either custom defined by the user or selected from a set of standard aerosols. The standard aerosol models available in MODTRAN-P used in this study are the standard rural aerosol with 23-km visibility, the standard urban aerosol with 5-km visibility, and the standard troposphere aerosol with 50-km visibility. Each standard aerosol model contains four typical extinction profiles for each of the four aerosol classes. MODTRAN allows the user to modify the standard aerosol models with user-defined extinction profiles. Besides the extinction profile, the user also may define phase matrices using Mie-generated functions, Henyey–Greenstein functions, or user-defined matrices.

For our purpose, aerosol extinction profile data were retrieved from solar radiometer and LIDAR data (see Sec. 2.2.1), while the aerosol phase matrix and wavelength dependence were selected by the standard models—rural 23 km, urban 5 km, or troposphere 50 km. Dependence of the model DoLP on the selection of these standard aerosol types is tested in the clear-sky models below. At the time of this study we were using a three-channel solar radiometer, although we now operate a nine-channel instrument from which aerosol size distributions and scattering phase matrices can be retrieved.[17] Although the three-channel radiometer did not allow such retrievals, it is expected that any model accuracy gained by improved scattering phase matrices will be limited until the multiple-scattering algorithms are implemented fully.[11]

Therefore, the standard MODTRAN models were used for the aerosol type, the standard MODTRAN Mie-generated models were used for the scattering phase matrix, and the extinction profile (described in Sec. 2.2.1) was obtained from combined LIDAR and three-channel solar radiometer data.

#### 2.2.1 Aerosol extinction profile retrieval from LIDAR and solar radiometer data

Optical depths at 425, 500, and 790 nm were obtained from measurements made with a solar radiometer that measured column-integrated solar extinction.[18] None of the solar radiometer wavelengths exactly matched the 550-nm extinction profile needed for MODTRAN. However, using the 425- and 500-nm data, the Angstrom exponent between these two optical depths was calculated and used to estimate the 550-nm optical depth from the 500-nm optical depth and the calculated Angstrom exponent.

Although the solar radiometer provided the optical depth for the entire atmospheric column, LIDAR data were used to provide vertical structure. We used a single-wavelength, dual-polarization, zenith-viewing LIDAR[19] to obtain relative backscatter profiles at 532 nm. Using the solar radiometer optical depth with the LIDAR backscatter signal, an aerosol extinction profile was retrieved with the Fernald–Klett inversion scheme.[20,21] The extinction retrieval requires several assumptions. First, an accurate representation of the molecular extinction profile must be available, because the retrieved extinction profile must be separated into its molecular and aerosol components. We used MODTRAN to find the molecular extinction profile using the standard MODTRAN mid-latitude summer model in conjunction with our measured

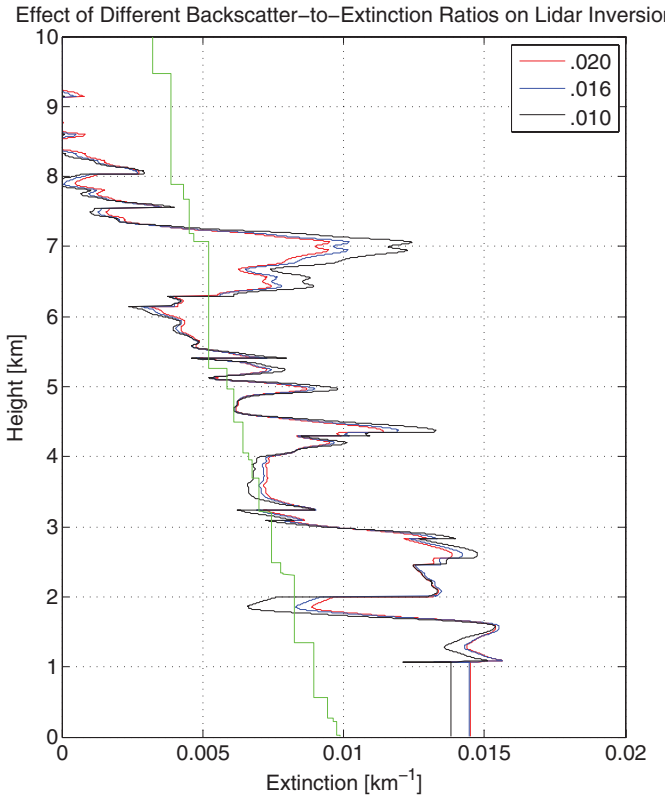


**Fig. 1** Effect on the aerosol extinction profile of varying the assumed aerosol background-to extinction ratio from 0.01 to 0.02.

radiosonde temperature, pressure, and humidity profiles (as discussed in Sec. 2.1). Second, the backscatter at 532 nm was assumed to be proportional to the backscatter at 550 nm. Third, the aerosol backscatter-to-extinction ratio must be known for the aerosols. Since we did not have information available for this value (from AERONET for example), the aerosol backscatter-to-extinction ratio for all clear-sky data was set to a typical value of 0.016 over the entire profile.[22] Although the backscatter-to-extinction ratio could vary slightly from this value, the optical depth bounded the LIDAR inversion. Errors in backscatter-to-extinction ratio did not affect the overall extinction derived for the column, but instead caused local variations in the aerosol extinction. Figure 1 shows the influence of varying the backscatter-to-extinction ratio between 0.020 and 0.010. Notice that there are some local variations with extinction, but in most regions the variation is minimal. Since MODTRAN coarsely samples aerosol profiles into 32 layers, these local errors are insignificant compared to the sampling errors. Also, we expect that the overall aerosol optical depth is a more important variable than the vertical structure of aerosol extinction.

On September 6, 2006, Bozeman experienced very thick forest fire smoke and it was apparent that the LIDAR did not penetrate the smoke layer. In this case, the extinction profile was modeled as the standard rural 23-km model above 3-km with the balance of the large optical depth spread homogenously over the lower 3 km of the column.

## *2.3 Miscellaneous MODTRAN-P Input Notes*

For all profiles—aerosol, molecular, and cloud—MODTRAN requires that the data be down-sampled to a maximum of 32 layers. One early discovery—although not surprising—was that

the stratosphere must be sampled adequately or the degree of polarization would change dramatically. Because light in the stratosphere experiences less multiple scattering and less aerosol scattering, it scatters more highly polarized light than the aerosol-laden troposphere. Because of its importance, at least 6 of the 32 layers were always reserved for the stratosphere in our models.

Although surface reflection can have a significant effect on atmospheric polarization,[22–24] this particular model cannot properly incorporate this effect because of the lack of polarized multiple scattering. Therefore, we used zero surface reflectance in all models. We are presently developing a quantitative relationship between surface reflectance and sky polarization using our sky polarization data and satellite surface reflectance data.

## 3 Clear-Sky Polarization Comparisons

Most of our research has centered on the accuracy of skylight DoLP, and especially the maximum of the DoLP. If the maximum DoLP (approximately 90° from the Sun) is not accurate, the polarization of other sky areas will follow suit. In this paper, we compare observed and modeled maximum DoLP. For both the model and the actual data, the maximum degree of polarization was found. After calculation of the polarization data from the raw data,[13,14] the DoLP image was filtered with a $5 \times 5$ median filter to remove artifacts and a maximum was taken. An iterative search algorithm found the maximum DoLP for the model. (The maximum model DoLP was always found to be within a few degrees of 90° from the solar zenith angle.)

The model was validated under three different cloud-free sky conditions: optically thin boundary-layer aerosols, slightly elevated optical-thickness boundary-layer aerosols, and optically thick boundary-layer aerosols. For all sky conditions, the daily-average of the total optical depth (OD) and aerosol optical depth (AOD) at 500 nm is given, and on days when the optical depth was on a similar scale as the maximum DoLP, it is plotted versus time.

For each aerosol thickness, MODTRAN-P was run with each of three different standard aerosol types—rural, urban, and tropospheric. Each of these models was run in both the polarized single-scattering mode and the polarized single-scattering plus unpolarized multiple-scattering mode. Since this version of MODTRAN-P models multiple scattering as exclusively unpolarized, multiple scatter models were expected to always predict a lower degree of polarization than reality.

Since the version of the MODTRAN-P code that we use here is a preliminary version, our study does not focus on the absolute accuracy of the model—and should not be interpreted as such—but instead focuses on the following questions: 1. How well do the shapes of the maximum DoLP models over each day compare to measurements? 2. How dependent are the model results on aerosol type? 3. Do any of the standard aerosol models appear adequate at our full range of optical depth? 4. How accurate is a single-scatter model and under what conditions is it valid?[25] For all plots in the following sections, the color of the plotted line closely represents the color corresponding to the wavelength of light for both maximum DoLP and total OD at 500 nm. Black represents the 700-nm wavelength. Solid lines without symbols represent measured data, while lines with symbols represent modeled results. Time is in Mountain Daylight Time (MDT = UTC-6 h). The optical depths listed in each section title are the total OD and AOD at 500 nm, representative of the values occurring each day.

### *3.1 Low Aerosol Content (OD ≈ 0.16, AOD ≈ 0.035)*

One of the clearest days of the year occurred on September 25, 2006. This day was chosen for comparisons under conditions with low aerosol content.

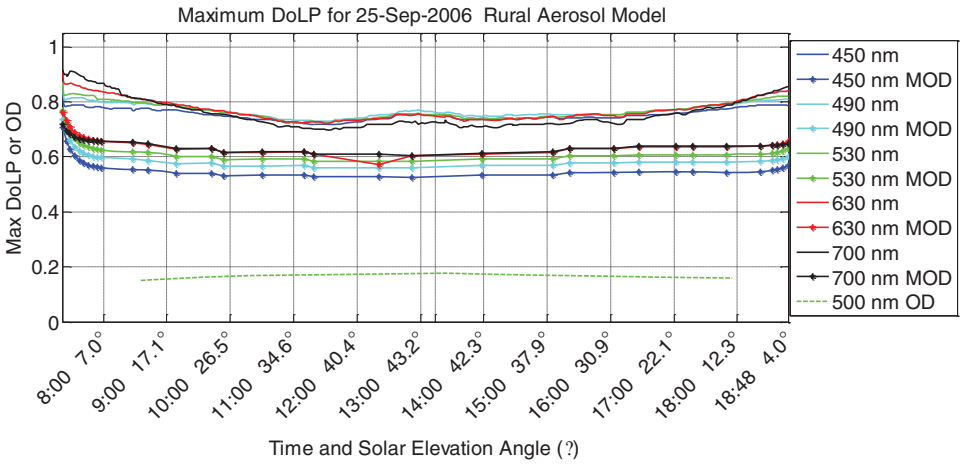


**Fig. 2** Low-aerosol max DoLP with rural aerosol multiple-scatter model. In this and subsequent plots, each wavelength is shown using a line color that is similar to the relevant wavelength. Solid lines with dot markers show the model results (MOD). The 500-nm total optical depth measured with the solar radiometer is shown with a green dashed line. The extra vertical line near the center marks the position of solar noon.

### *3.1.1 Rural aerosol models*

Rural aerosol model comparisons are shown in Fig. 2 for the multiple-scatter model and in Figs. 3 and 4 for the single-scatter model. Notice that the multiple-scatter models better preserve the shape of the maximum DoLP curve over the day, especially for the longer wavelengths. Still, the models consistently underpredict the maximum DoLP and exhibit a larger spread across wavelengths than the measured data. Also, the 700-nm measurements exhibit the highest DoLP near sunrise and sunset, while in the model the 630-nm data are slightly higher.

For the single-scatter rural aerosol models, all model results are much closer to the measurements than their multiple-scatter counterparts, with maximum errors around 13% for the short wavelengths (Figs. 3 and 4). The shape of the maximum DoLP curve as a function of solar elevation angle (or time) also tracks well. During mid-day readings, both the 630- and the 700-nm models and measurements are within the instrument accuracy. Still, near sunrise and sunset the model severely underpredicts the maximum DoLP by up to 13%. (This is related at

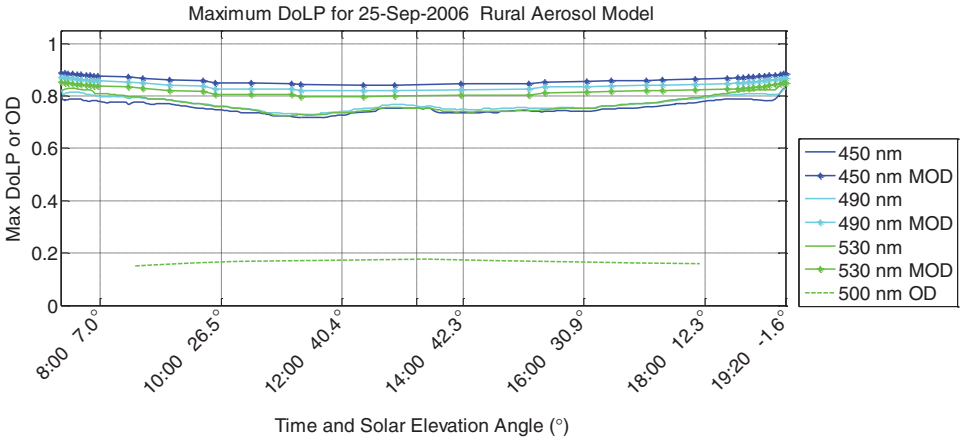


**Fig. 3** Low-aerosol maximum DoLP with rural single-scatter model for 450 to 530 nm.

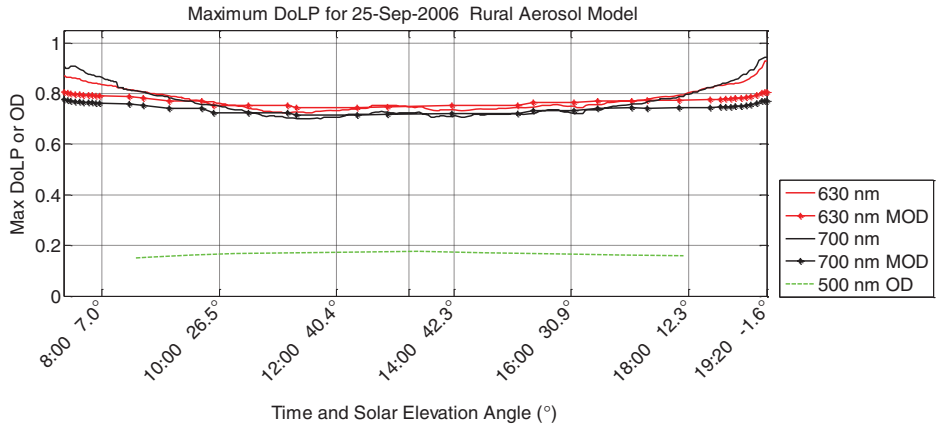


**Fig. 4** Low-aerosol maximum DoLP with rural single-scatter model for 630 to 700 nm.

least partially to the inability of a plane-parallel radiative transfer code to model realistic results for large solar zenith angles.)

### *3.1.2 Urban aerosol models*

Urban multiple-scatter models exhibit maximum DoLPs that are nearly identical to the rural aerosol model, except with a 4% shift toward the instrument data (Fig. 5). This may suggest a better correlation between the urban aerosol model and the forest fire smoke seen in the Gallatin valley during September than the rural aerosol model. Still, urban single-scatter models also increased by about 4% for the long wavelengths and about 2% for the shorter wavelengths from the rural cases. This increase pulls the urban single-scatter models away from the actual data (Figs. 6 and 7).

### *3.1.3 Tropospheric aerosol models*

For most MODTRAN standard models, the boundary layer (<3 km) uses the standard aerosol (urban, rural, maritime, etc.), while the troposphere above the boundary layer uses the standard tropospheric aerosol. In the standard tropospheric model, the tropospheric aerosol type is extended through the boundary layer. Although it may not be as representative as the urban or rural

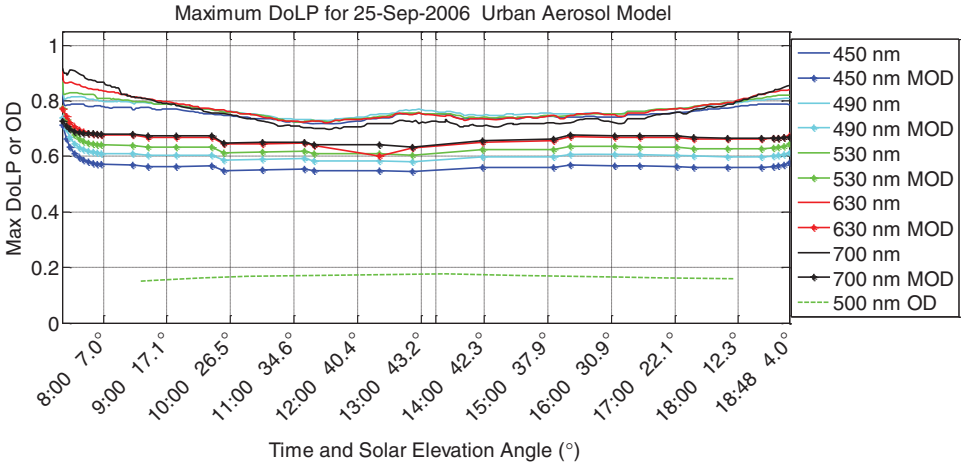


**Fig. 5** Low-aerosol maximum DoLP with urban aerosol multiple-scatter model.

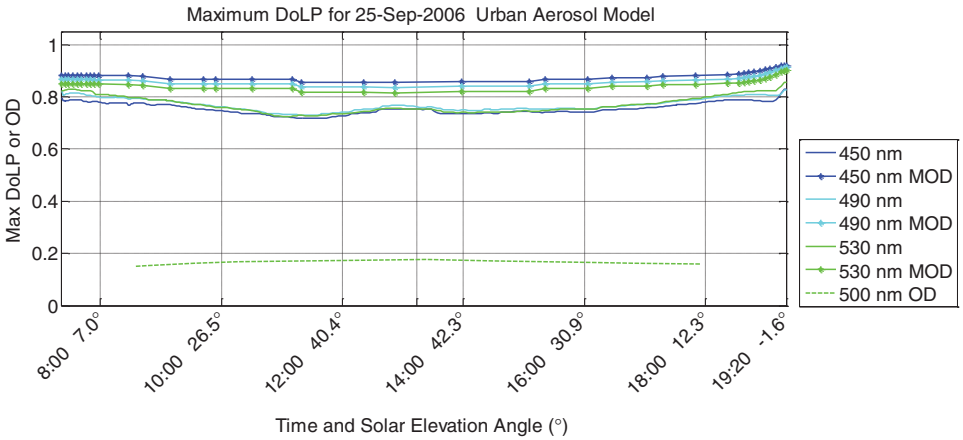


**Fig. 6** Low-aerosol maximum DoLP with urban single-scatter model for 450 to 530 nm.

aerosols, this model is included as an alternative. Compared to the other two multiple-scatter models, the tropospheric aerosol type bunches the wavelengths in a more realistic way, but the overall accuracy of the model decreases by ~5% from the rural model (Fig. 8). For the clear sky, this is the worst model with multiple scattering.

For the single-scatter models, the shorter wavelengths move the DoLP about 1.5% lower than the rural model, while the longer wavelengths remain below the instrument data (Figs. 9 and 10). Similar results were seen for the tropospheric aerosol models for the moderate and high aerosol content comparisons. For brevity, these results are not reported here, but can be found elsewhere.[26]

### *3.2 Moderate Aerosol Content (OD ≈ 0.22, AOD ≈ 0.095)*

In August and September 2006, fires burned throughout Montana. In particular, fires burned in the Paradise Valley southeast of Bozeman in early September. These fires created extremely low visibility on September 5, 2006 (see Sec. 3.3 for data from this day). By September 11, the smoke had cleared considerably. This day provided moderate aerosol data.

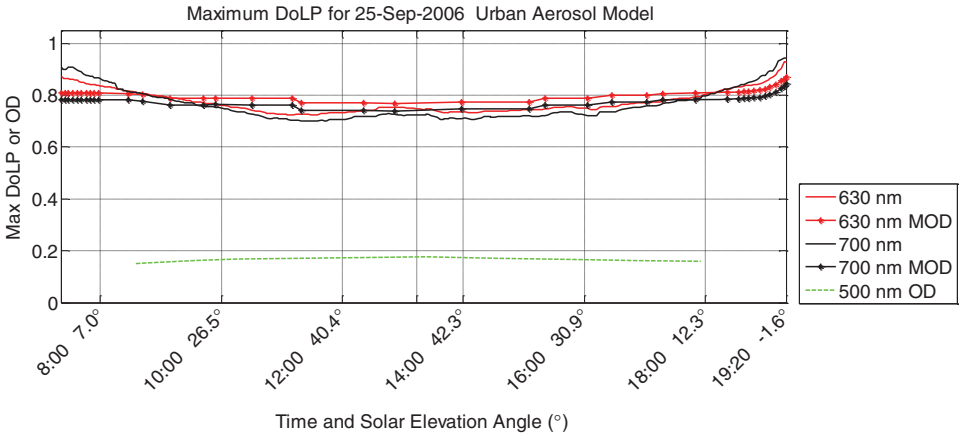


**Fig. 7** Low-aerosol maximum DoLP with urban single-scatter model for 630 to 700 nm.

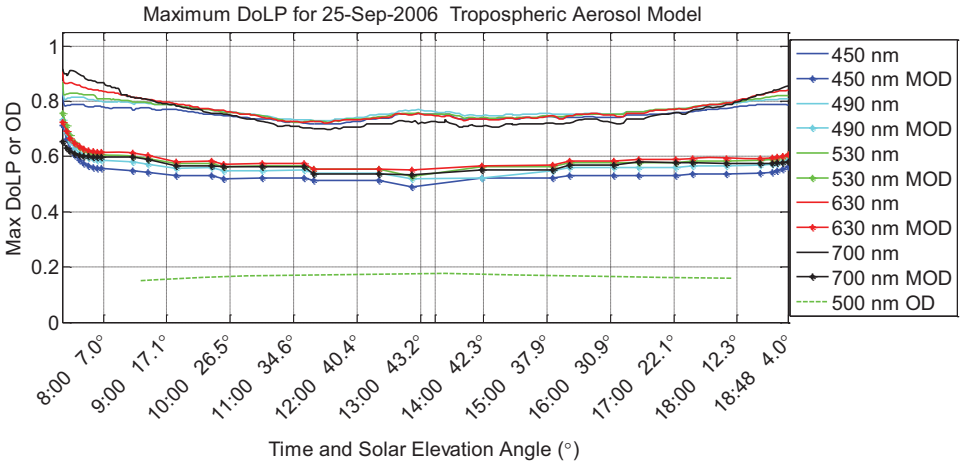


**Fig. 8** Low-aerosol maximum DoLP with tropospheric aerosol multiple-scatter model.

### *3.2.1 Rural aerosol models*

Figure 11 shows the results of the rural aerosol model with multiple scattering. For this day, the AOD dropped during the course of the afternoon, causing a concurrent upward trend in the DoLP when compared to the morning. The model tracks this trend appropriately. Still, multiple-scatter models consistently underpredict the DoLP.

With moderate aerosols, single-scatter models overpredict the DoLP for all wavelengths (Figs. 12 and 13). This is a departure from the low-aerosol rural models, which predict the longer wavelengths well. For the mid-day clear sky, a single-scatter model seems to be adequate for the longer wavelengths, but as aerosols increase, the scattering in the boundary layer causes the model to separate from the actual data. Notice that as the optical depth at 500 nm begins to drop below 0.20, the single-scatter 630- and 700-nm models agree with measurement to within the instrument error, but above this optical depth they diverge.

### *3.2.2 Urban aerosol models*

Comparisons of measurements with the urban aerosol model are shown in Figs. 14–16. For the multiple-scatter model the results are almost identical to the rural model—except 1% lower.

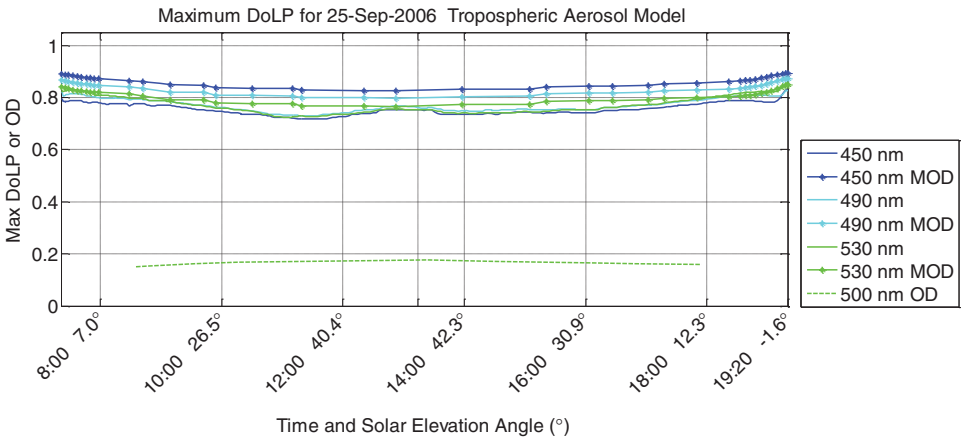


**Fig. 9** Low-aerosol maximum DoLP with tropospheric single-scatter model for 450 to 530 nm.

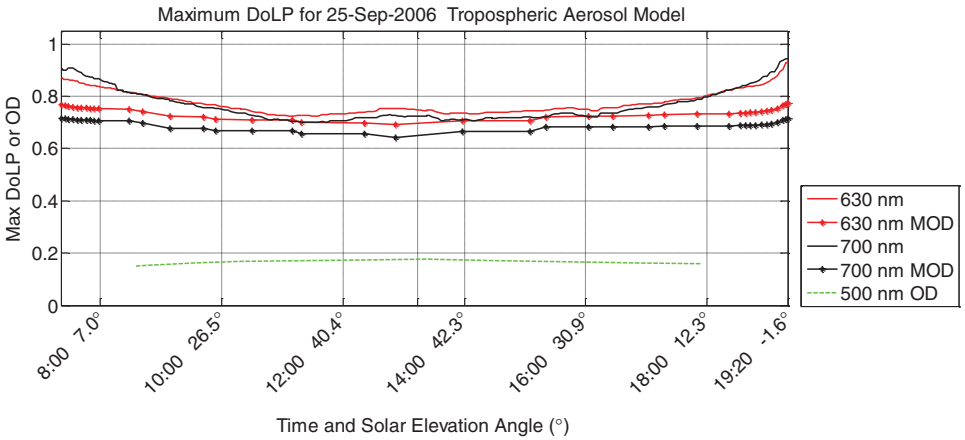


**Fig. 10** Low-aerosol maximum DoLP with tropospheric single-scatter model for 630 to 700 nm.

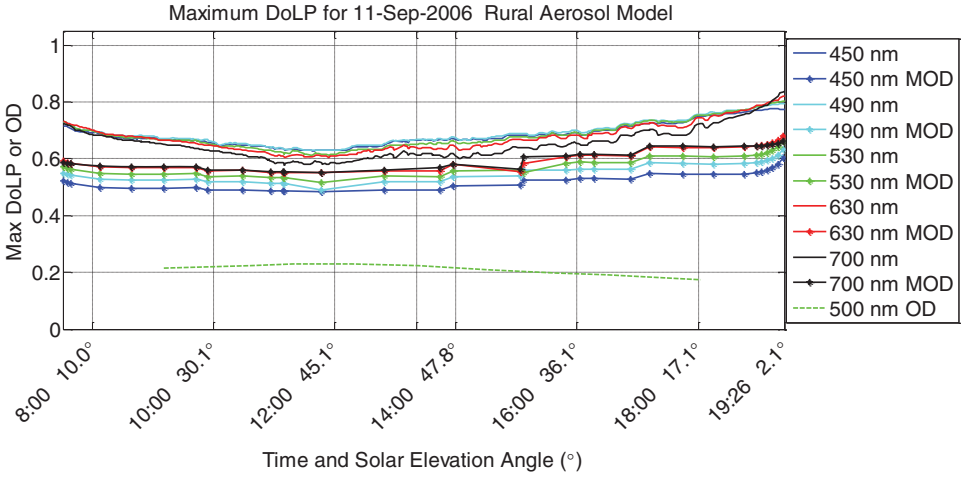


**Fig. 11** Moderate-aerosol maximum DoLP with rural aerosol multiple-scatter model.

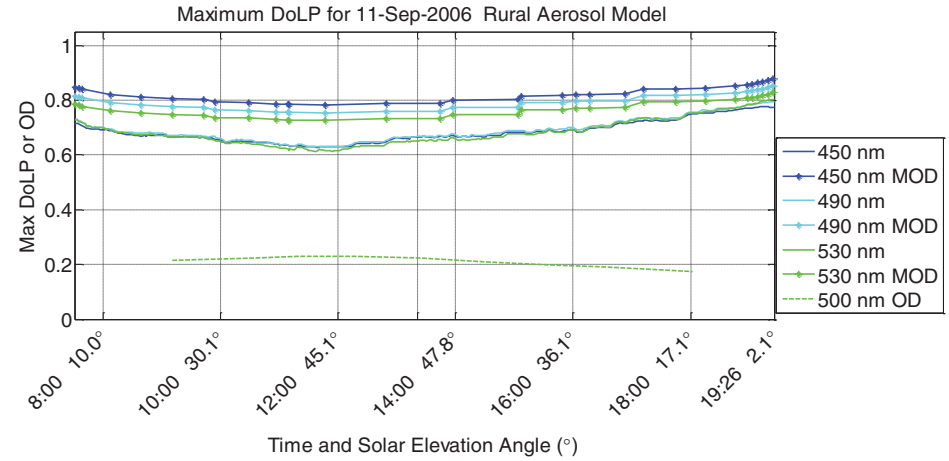


**Fig. 12** Moderate-aerosol maximum DoLP with rural single-scatter model for 450 to 530 nm.

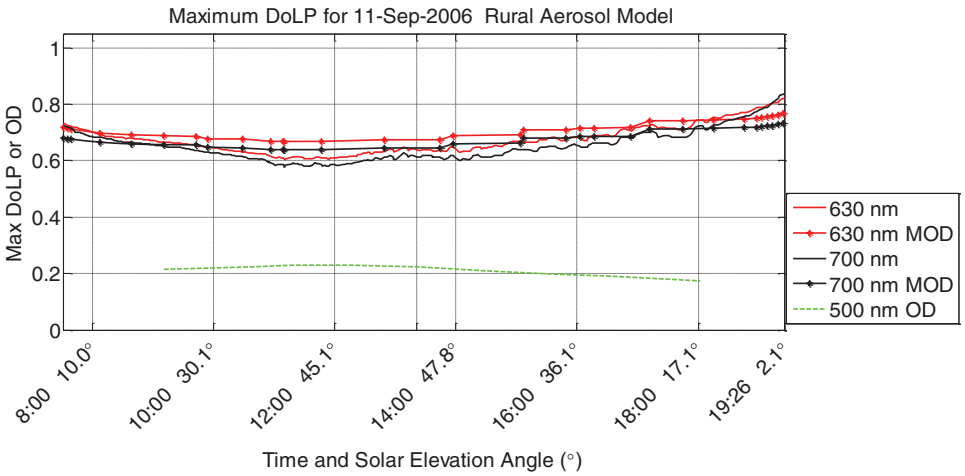


**Fig. 13** Moderate-aerosol maximum DoLP with rural single-scatter model for 630 to 700 nm.

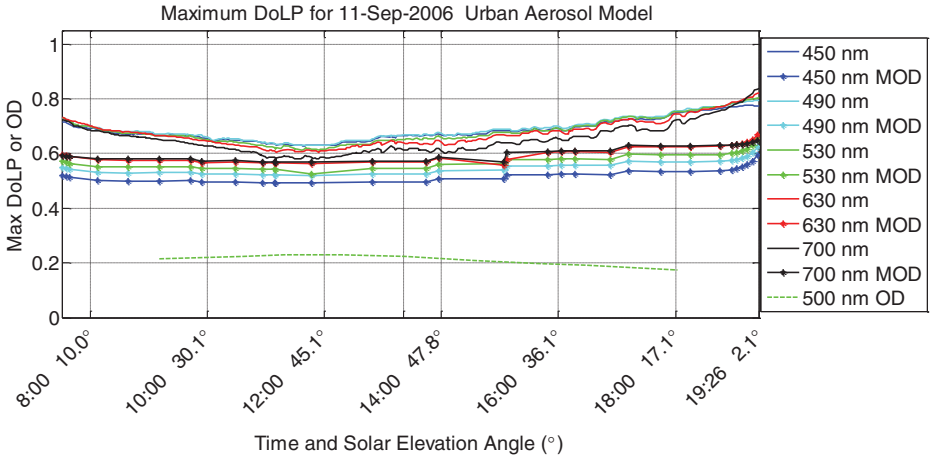


**Fig. 14** Moderate-aerosol maximum DoLP with urban aerosol multiple-scatter model.

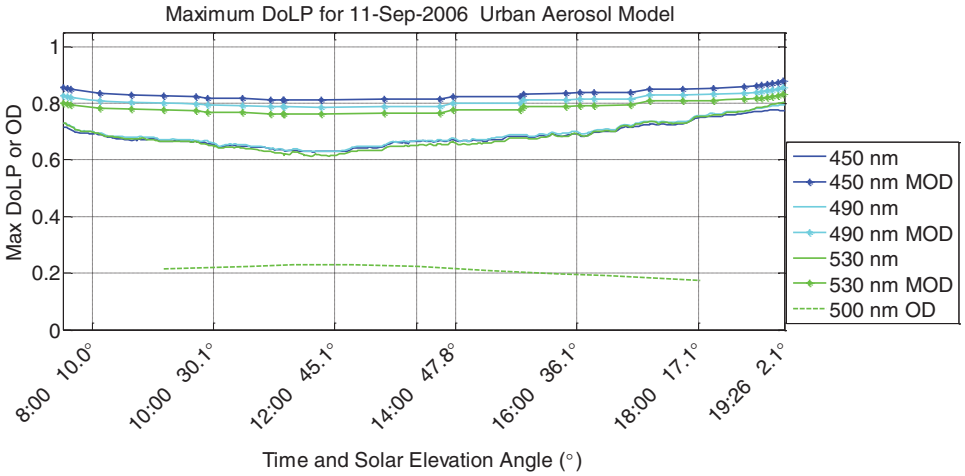


**Fig. 15** Moderate-aerosol maximum DoLP with urban single-scatter model 450 to 530 nm.

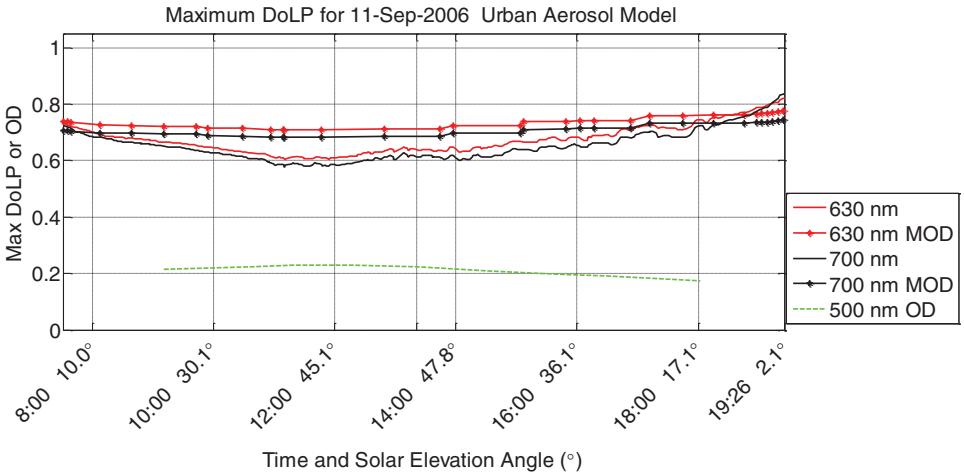


**Fig. 16** Moderate-aerosol maximum DoLP with urban single-scatter model 630 to 700 nm.

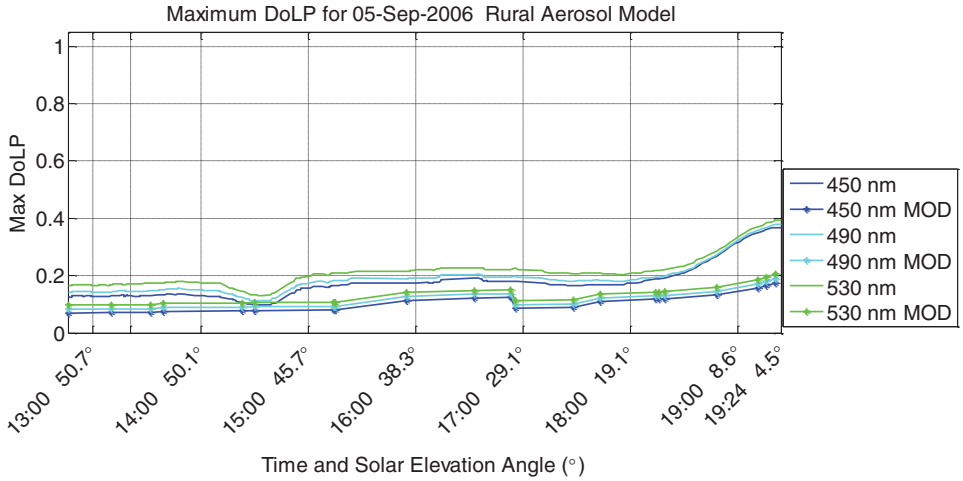


**Fig. 17** High-aerosol maximum DoLP with rural multiple-scatter model for 450 to 530 nm.

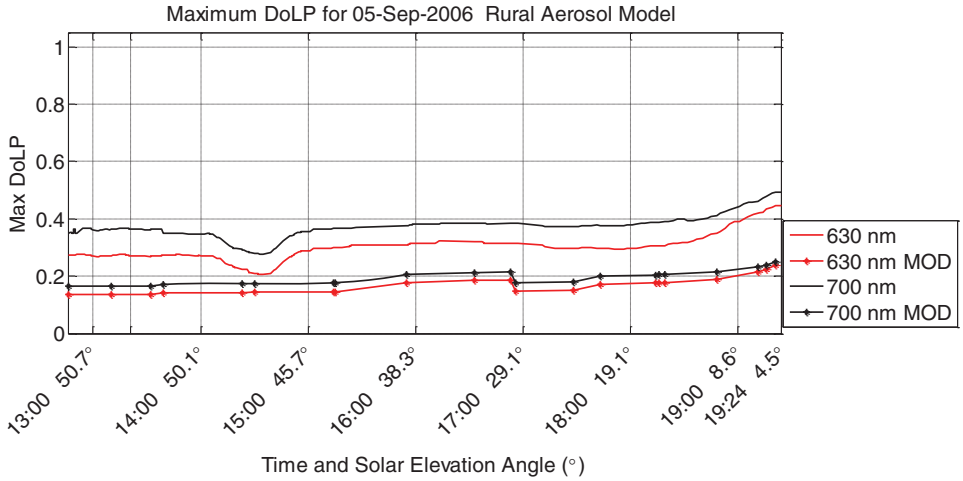


**Fig. 18** High-aerosol maximum DoLP with rural multiple-scatter model for 630 to 700 nm

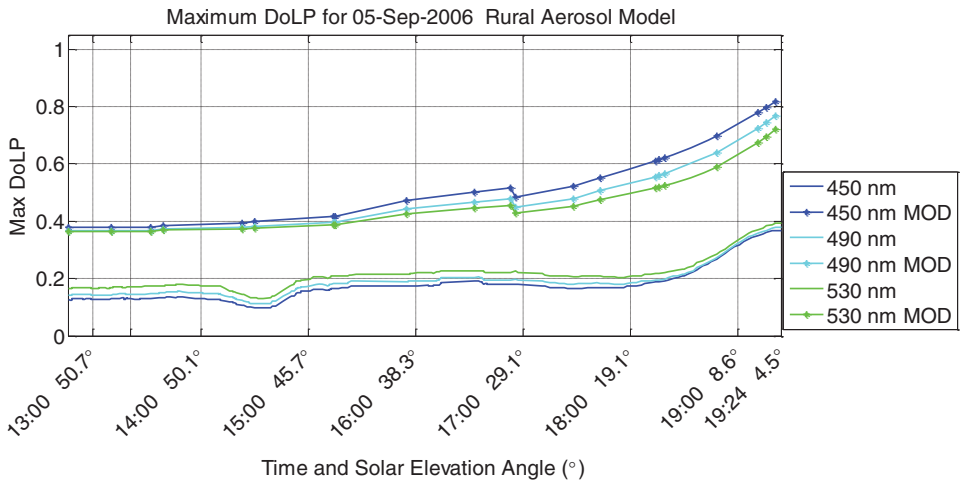


**Fig. 19** High-aerosol maximum DoLP with rural single-scatter model for 450 to 530 nm.

The single-scatter urban models are similar to their rural counterparts, but in all cases they overpredict the measured DoLP to a larger extent than the rural models.

## *3.3 High Aerosol Content (OD ≈ 1.2, AOD ≈ 1.075)*

A very dense aerosol layer from a nearby forest fire occurred on September 5, 2006. At some points in the afternoon, visibility on the ground was below 1.5 km. Only afternoon data were taken on this day. The dip in the measured maximum DoLP around 14:30 is from clouds that formed in the early afternoon. These clouds can be seen in the polarimeter images around this time. It appears from the polarimeter images that even the thinnest clouds went away later in the afternoon, but visibility was bad enough that we had to turn to satellite images to confirm that this was generally the case. The optical depth (not shown in the figures since it is off scale) slowly moved from 1.34 at 12:50 to 1.00 at 16:39. Later in the day it slowly increased to 1.25 at 18:10.

### *3.3.1 Rural aerosol models*

Comparisons of measurements with the multiple-scatter models for the high-aerosol day are shown in Figs. 17 and 18. For clarity, the shorter wavelengths are plotted in a separate figure from the longer wavelengths. The multiple-scattering model consistently underpredicts the DoLP. During mid-day, the long-wavelength errors are separated from the observed data by as much as 20%, while the shorter wavelengths differ by 10%.

Single-scatter models exhibit characteristics similar to the other models, but with more extreme differences between measurements and model results. Short wavelengths are not even similar (Fig. 19). Surprisingly, the largest error in the 700-nm wavelength model is only 6% (Fig. 20).

### *3.3.2 Urban aerosol models*

The same series of comparisons were made with the urban aerosol model, with results similar to, and even somewhat worse, than those for the rural aerosol model (these results are not plotted in the interest of space but can be found elsewhere[26]). For all urban multiple-scatter models with high aerosol content, measured and calculated data were within 6%, except near sunset. These short-wavelength urban cases are the only instances across all the models for which the

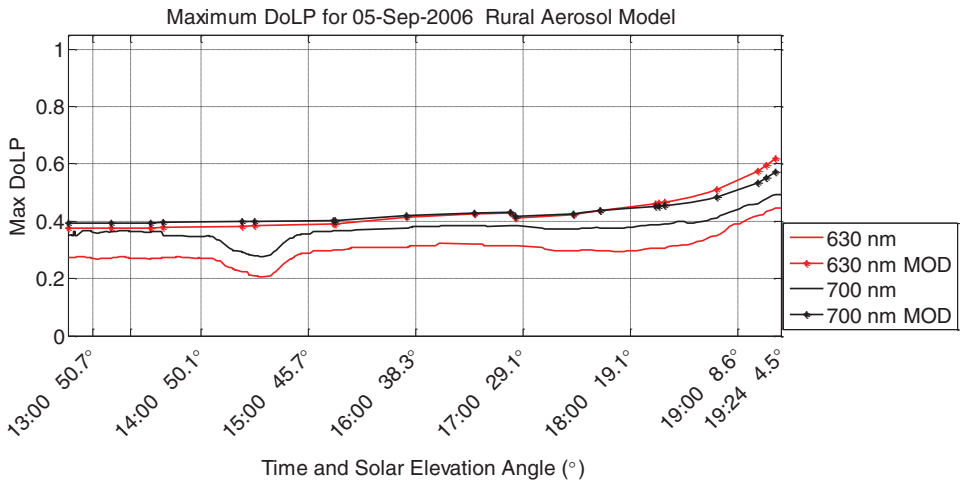


**Fig. 20** High-aerosol maximum DoLP with rural single-scatter model for 630 to 700 nm.

multiple-scatter model is above the measured DoLP. Since the multiple scattering is modeled without polarization, all model results should be below the measured data. This suggests either that the urban aerosol model is not a good representation of the September 5 forest fire aerosols or that this preliminary implementation of multiple scatting in MODTRAN-P is not sufficient. As with the rural models, the single-scatter urban models always disagree significantly from measurements in a manner similar to the rural model comparisons. These results reinforce the need for more detailed information about the aerosol size distribution and optical properties for a complete validation of polarized simulations.

## 4 Discussion and Conclusions

The maximum DoLP of skylight has been compared with MODTRAN-P simulations for a variety of cloud-free sky conditions. For optical depths less than 0.20, mid-day single scatter models are adequate for 630 and 700 nm. This is reasonable, since the longer wavelengths are less affected by multiple scattering in a cleaner atmosphere. The preliminary MODTRAN-P multiple-scatter model consistently underpredicts the DoLP for all wavelengths, presumably because the multiple scattered component is modeled without polarization. Nevertheless, the unpolarized multiple-scatter model performs better than the polarized single-scatter model at maintaining an appropriate curve shape during sunrise and sunset. The single-scatter models consistently underpredict the long wavelength DoLPs for low-aerosol skies at sunrise and sunset. These results show that for situations with anything more than the smallest amount of aerosol scattering, both the single-scatter and the single-scatter plus unpolarized multiple-scattering approximations are not adequate. This restricts the utility of this preliminary version of the MODTRAN-P code. A more complete implementation is needed.

The accuracy of each model depends greatly on the type of aerosol used in the model. For high-aerosol conditions, the difference between models using different standard aerosol types can be as much as 20% DoLP. For low-aerosol conditions, the difference between models can be as much as 10% DoLP. It is apparent that the most meaningful comparison of a polarized radiative transfer model with measurements should not rely on standard aerosol models, but should instead incorporate the best available measurements or retrievals of aerosol size distribution and refractive index. These aerosol parameters can be used with Mie scattering codes to create an aerosol scattering phase matrix to be used in a radiative transfer model. Our approach to satisfying this need was to obtain and install a multiwavelength solar radiometer for determining aerosol size distributions and aerosol optical properties.

## Acknowledgments

We thank Dr. Glenn Shaw of the University of Alaska–Fairbanks for providing a solar radiometer used in this study.

This material is based on research sponsored by the Air Force Research Laboratory, under agreement no. FA9550–07-1–0011. The U.S. Government is authorized to reproduce and distribute reprints for Governmental purposes notwithstanding any copyright notation thereon. The views and conclusions contained herein are those of the authors and should not be interpreted as necessarily representing the official policies or endorsements, either expressed or implied, of the Air Force Research Laboratory or the U.S. Government.

## References

1. J. S. Tyo, D. L. Goldstein, D. B. Chenault, and J. A. Shaw, "A review of passive imaging polarimetry for remote sensing applications," *Appl. Opt.* **45**(22), 5453–5469 (2006).
2. M. I. Mishchenko, B. Cairns, G. Kopp, C. F. Schueler, B. A. Fafaul, J. E. Hansen, R. J. Hooker, T. Itchkawich, H. B. Maring, and L. D. Travis, "Accurate monitoring of terrestrial aerosols and total solar irradiance: Introducing the glory mission," *Bull. Am. Meteorol. Sci.* **88**, 677–691 (2007).
3. J. L. Deuze, M. Herman, P. Goloub, D. Tanre, and A. Marchand, "Characterization of aerosols over ocean from POLDER/ADEOS-1," *Geophys. Res. Lett.* **26**(10), 1421–1424 (1999).
4. Z. Li, P. Goloub, O. Dubovik, L. Blarel, W. Zhang, T. Podvin, A. Sinyuk, M. Sorokin, H. Chen, B. Holben, D. Tanre, M. Canini, and J.-P. Buis, "Improvements for ground-based remote sensing of atmospheric aerosol properties by additional polarimetric measurements," *J. Quant. Spec. Rad. Trans.* **110**(17), 1954–1961 (2009).
5. J. A. Shaw, "Degree of linear polarization in spectral radiances from water-viewing infrared radiometers," *Appl. Opt.* **38**(15), 3157–3165 (1999).
6. J. A. Shaw, "A survey of infrared polarization in the outdoors," *Proc. SPIE* **6660**, 666006 (2007).
7. K. Coulson, *Polarization and Intensity of Light in the Atmosphere*, Deepak, Hampton, VA (1988).
8. A. Berk, G. P. Anderson, P. K. Acharya, L. S. Bernstein, L. Muratov, J. Lee, M. Fox, S. M. Adler-Golden, J. H. Chetwynd Jr., L. M. Hoke, R. B. Lockwood, J. A. Gardner, T. W. Cooley, C. C. Borel, P. E. Lewis, and E. P. Shettle, "MODTRAN5: 2006 update," *Proc. SPIE* **6233**, 62331F (2006).
9. M. P. Fetrow, D. Wellems, S. H. Sposato, K. P. Bishop, T. R. Caudill, M. L. Davis, and E. R. Simrell, "Results of a new polarization simulation," *Proc SPIE* **4481**, 149–162 (2002).
10. M. Fetrow, personal correspondence, Air Force Research Laboratory, Albuquerque, NM (2006).
11. M. Hoke, personal correspondence, Air Force Research Laboratory, Hanscom Air Force Base, MA (2010).
12. C. Devaraj, S. Brown, D. Messinger, A. Goodenough, and D. Pogorzala, "A framework for polarized radiance signature prediction for natural scenes," *Proc. SPIE* **6565**, 65650Y (2007).
13. N. J. Pust and J. A. Shaw, "Dual-field imaging polarimeter using liquid crystal variable retarders," *Appl. Opt.* **45**, 5470–5478 (2006).
14. N. J. Pust and J. A. Shaw, "Digital all-sky polarization imaging of partly cloudy skies," *Appl. Opt.* **47**(34), H190–H198 (2008).
15. A. Bucholtz, "Rayleigh scattering calculations for the terrestrial atmosphere," *Appl. Opt.* **34**, 2765–2773 (1995).

16. G. P. Anderson, S. A. Clough, F. X. Kneizys, J. H. Chetwynd, and E. P. Shettle, "AFGL atmospheric constituent profiles (0–120 km)," Air Force Geophysics Laboratory Environmental Research Papers No. 954, AFGL-TR-86-0110 (1986).
17. B. N. Holben, T. F. Eck, I. Slutsker, D. Tanre, J. P. Buis, A. Setzer, E. Vermote, J. A. Reagan, Y. J. Kaufman, T. Nakajima, F. Lavenu, I. Jankowiak, and A. Smirnov, "AERONET—a federated instrument network and data archive for aerosol characterization," *Remote Sens. Env.* **66**, 1–15 (1998).
18. G. E. Shaw, "Sun photometry," *Bull. Am. Meteor. Soc.* **64**, 4–10 (1983).
19. N. L. Seldomridge, J. A. Shaw, and K. S. Repasky, "Dual-polarization lidar using a liquid crystal variable retarder," *Opt. Eng.* **45**, 106202 (2006).
20. F. G. Fernald, B. M. Herman, and J. A. Reagan, "Determination of aerosol height distribution by lidar," *J. Appl. Meteorol.* **11**, 482–489 (1972).
21. J. D. Klett, "Stable analytical inversion solution for processing lidar returns," *Appl. Opt.* **20**, 211–220 (1981).
22. V. A. Kovalev, W. E. Eichinger, *Elastic Lidar*, Wiley-Interscience, New York, Table 7.1 (2004).
23. A. R. Dahlberg, N. J. Pust, and J. A. Shaw, "All-sky imaging of visible and NIR skylight at Mauna Loa," *Proc. SPIE* **7461**, 746107 (2009).
24. A. R. Dahlberg, "All-sky polarization imager deployment at Mauna Loa Observatory, Hawaii, M. S. Thesis, Montana State University (2010) [http://etd.lib.montana.edu/etd/view/item.php?id=1048].
25. N. J. Pust and J. A. Shaw, "How good is a single-scattering model of visible-NIR atmospheric skylight polarization?," *Proc. SPIE.* **7461**, 74610B (2009).
26. N. J. Pust, "Full sky imaging polarimetry for initial polarized MODTRAN validation," PhD Dissertation, Montana State University (2007) [http://etd.lib.montana.edu/etd/view/item.php?id=489].

**Nathan J. Pust** is a research engineer working at Montana State University. He received Bachelor's degrees in electrical engineering and computer engineering from Montana State University in 2002, and his PhD in electrical engineering from Montana State University in 2007.

**Joseph A. Shaw** is a professor in the electrical and computer engineering department and the director of the Optical Technology Center at Montana State University in Bozeman, Montana. He received a PhD and MS in optical sciences from the University of Arizona in 1996, a Master of Science in electrical engineering from the University of Utah in 1989, and a Bachelor of Science in Electrical Engineering from the University of Alaska – Fairbanks in 1987. He is a Fellow of OSA and SPIE.